Computationally and Energy Efficient Symbol-Level Precoding Communications Demonstrator

Jevgenij Krivochiza, J.C. Merlano-Duncan, Stefano Andrenacci, Symeon Chatzinotas, Björn Ottersten

SnT, SigCom
29 Avenue JF Kennedy
L-1855, Luxembourg

Abstract

We demonstrate forward link interference mitigation techniques in a precoded multi-user communication scenario for the efficient frequency reuse. The developed test-bed provides an end-to-end precoding demonstration, which includes a transmitter, a multi-beam satellite channel emulator and user receivers. Precoded communications allow efficient frequency reuse in multiple-input multiple-output (MIMO) channel environments, where several coordinated antennas simultaneously transmit to a number of independent receivers. We implement and demonstrate the new Symbol-Level Precoding (SLP) technique and benchmark it against Zero-Forcing and MMSE techniques in realistic transmission conditions. We show performance of the SLP in various MIMO channel conditions and outline the impact of the modified constellation by the SLP on a conventional receiver.

Keywords: MIMO, precoding, beamforming, SNR, BER, convex optimization, power minimization, multi-user interference

1. Introduction

Multi-User MIMO (MU-MIMO), also known as Precoding, has been studied recently as a way to reduce co-channel interference in the wireless communications (Wi-Fi, LTE) and multi-beam satellite systems [1, 2, 3, 4]. The requirement of broadband services through high throughput satellite (HTS) systems motivated the research of advanced signal processing techniques for interference mitigation to provide a better spectrum utilization with a reasonable complexity. MU-MIMO communication techniques are also promissory in other multi-channel interference scenarios such as in the case of Asymmetric digital subscriber line [5] (ADSL) and Powerline communications [6].

Email address: jevgenij.krivochiza@uni.lu (Jevgenij Krivochiza)

The approach to this challenge is the use of the aforementioned precoding techniques, which allow aggressive reuse of the frequency spectrum by exploiting the spatial multiplexing. The conventional channel-based Precoding techniques use the knowledge of the Channel State Information (CSI) in order to generate the transmitted precoded signals. The most common channel-based strategies are the channel inversion, also known as Zero Forcing (ZF), and the Minimal Means Square Error (MMSE) method [7]. These methods were studied and extended in the recent works with the focus on power optimization issue [8, 9]. More advanced approaches also use the knowledge of the intended transmitted symbols, in addition to the CSI, in order to obtain an optimal set of precoded symbols per each transmission time slot.

The challenge behind hardware implementations is to design realistically feasible precoder algorithm in terms of computational complexity, while facing real impairments over the communication link. Despite that numerous theoretical publications on symbol-level precoding techniques have appeared recently [10, 11, 12], practical feasibility was out of their scope.

Last year, the SIGCOM (Signal Processing) Research group from the University of Luxembourg has started to build a Satellite Precoding Hardware demonstrator for full frequency reuse named SERENADE [13]. The demonstrator includes symbol-level precoding (SLP) techniques, which optimize the beamforming vectors per every transmitted set of symbols. This leads to improving Signal-to-overall-Noise ratio, service availability and energy efficiency.

In this extended paper of work published in [14], we extend the description of the complexity of the novel SLP Precoder. We demonstrate theoretically and experimentally benefits of the Precoder in terms of energy and computationally efficiency. Towards this objective, we more thorough describe the practical implementation aspects of the hardware demonstrator, which consist of: a MIMO transmitter with capability to perform real-time SLP algorithm, a MIMO satellite channel emulator, and a set of receivers with CSI estimation capabilities. We estimate the optimal use cases of the SLP Precoder in such system.

We demonstrate an important connection between the condition number of the MIMO channel matrix and the performance of the SLP technique. The results shows, that the SLP can perform better than ZF at the particular channel matrix conditions, while for some channel matrices the performance of ZF and the SLP is the same.

We present practical issues and its solutions towards utilizing the SLP techniques in the receiver side. We discuss the impact of the SLP precoding algorithm on the symbol constellation and synchronization and demodulation issues with a conventional receiver, which influence the actual Quality of Service. To the best author's knowledge, the presented results have been never before studied in the literature and bring a significant insight on the SLP application in communications.

The rest of this paper is organized as follows. In Section 2, we state the system model, describe the precoding algorithms and analyze the computational efficiency. In Section 3, we evaluate the performance of the presented precoding technique in a simulated environment and compare the performance to a

benchmark techniques. In Section 4, we present experimental validation and analyze the experimental results of the precoding algorithm. Finally, we draw conclusions in Section 5. *Notation*: Upper-case and lower-case bold-faced letters are used to denote matrices and column vectors. The superscripts $(\cdot)^H$ and $(\cdot)^{-1}$ represents Hermitian matrix and inverse operations. $\|\cdot\|_2$ is the Euclidean norm, $|\cdot|$ is the absolute value of a complex, $\mathbf{0}$ is the all zero vector, and trace is the sum of all diagonal elements of a matrix. The real and imaginary parts of a complex value are defined as $\mathrm{Re}(\cdot)$ and $\mathrm{Im}(\cdot)$.

2. Symbol-Level Precoding Design

2.1. System Model

The general system model focuses on the forward link of a multi-beam satellite system, which aims at reusing the total available bandwidth among all beams of the coverage. We define the number of transmitting antenna elements as N_t and the total number of users as N_u in the coverage area. In the specified MIMO channel model, the received signal at the i-th user is $y_i = \mathbf{h}_i^\dagger \mathbf{x} + n_i$, where $\mathbf{h}_i^\dagger$ is a $1 \times N_t$ vector representing the complex channel coefficients between the i-th user and the N_t antennas of the transmitter, $\mathbf{x}$ is defined as the $N_t \times 1$ vector of the transmitted symbols at a certain symbol period and n_i is the independent complex circularly-symmetric (c.c.s.) independent identically distributed (i.i.d) zero mean Additive White Gaussian Noise (AWGN) measured at the i-th user's receive antenna. Assuming a system having $N_t = N_u = N$, which is the present case, looking at the general formulation of the received signal, which include the whole set of users, the linear signal model is:

$$\mathbf{y} = \mathbf{H}\mathbf{x} + \mathbf{n} = \mathbf{H}\mathbf{W}\mathbf{s} + \mathbf{n} \tag{1}$$

wd In this scenario, we define the linear precoding matrix $\mathbf{W} \in \mathbb{C}^{N \times N}$ which maps information symbols $\mathbf{s}$ into precoded symbols $\mathbf{x}$.

2.2. Precoding technique

We implemented the Low-Complexity Symbol-Level precoding technique [15] into the demonstrator among side the Zero-Forcing technique [7]. The essential difference from the ZF precoding method is the optimization vector $\mathbf{u} \in \mathbb{C}^N$, which is recalculated per every symbol set $\mathbf{s}$ to construct optimal precoded signal as

$$\mathbf{x} = \mathbf{W}_{\mathrm{ZF}}(\sqrt{\gamma}\mathbf{s} + \mathbf{u}), \tag{2}$$

where $\mathbf{W}_{\mathrm{ZF}} = \hat{\mathbf{H}}^H \cdot (\hat{\mathbf{H}} \cdot \hat{\mathbf{H}}^H)^{-1}$ is a Zero-Forcing precoding matrix, $\hat{\mathbf{H}} \in \mathbb{C}^{N \times N}$ - a channel matrix estimated from CSI and $\sqrt{\gamma}$ - the SNR requirement. The vector $\mathbf{u}$ adds a positive excursion to the user symbols $\mathbf{s}$. The excursion is always increasing the amplitude of the symbols. It is calculated for each set of symbols to increase signal-to-noise ratio (SNR) at the receiver side due to optimally preserved constructive interference components, which occur in the

MIMO channel. This effect decreases the total power of the precoded transmission signal $\mathbf{x}$ at the transmitter side. We define a convex optimization problem to minimize $\|\mathbf{x}\|_2$ with the SNR constrain as

$$\begin{array}{l} \min\limits_{\mathbf{u}} \|\mathbf{x}\|_2 \\ \text{s. t.} |\mathbf{y}| \geq |\mathbf{s}| \end{array}, \tag{3}$$

for $\mathbf{H}\mathbf{W}_{\text{ZF}} = \mathbf{I}$ and $\mathbf{n} = \mathbf{0}$. It was shown in [15], that the problem (3) can be transformed into a non-negative least squares (NNLS) problem as

$$\begin{array}{ll} \min\limits_{\tilde{\mathbf{u}}} & \|\widetilde{\mathbf{W}}_{\text{ZF}}\mathbf{B}\tilde{\mathbf{u}} - \mathbf{d}\|_2 \\ \text{subject to} & \tilde{\mathbf{u}} \geq 0 \end{array}, \tag{4}$$

where $\mathbf{d} = -\widetilde{\mathbf{W}}_{\text{ZF}}(\sqrt{\gamma}\tilde{\mathbf{s}})$, $\widetilde{\mathbf{W}} = [\text{Re}(\mathbf{W}_{\text{ZF}}), -\text{Im}(\mathbf{W}_{\text{ZF}}); \text{Im}(\mathbf{W}_{\text{ZF}}), \text{Re}(\mathbf{W}_{\text{ZF}})]$, $\tilde{\mathbf{s}} = [\text{Re}(\mathbf{s}^T), \text{Im}(\mathbf{s}^T)]^T$, $\tilde{\mathbf{u}} = [\text{Re}(\mathbf{u}^T), \text{Im}(\mathbf{u}^T)]^T$, and $\mathbf{B}$ is a diagonal matrix defined as:

$$\mathbf{B} = \begin{bmatrix} \tilde{s}_1/|\tilde{s}_1| & & \\ & \ddots & \\ & & \tilde{s}_N/|\tilde{s}_N| \end{bmatrix}. \tag{5}$$

If a solution for a particular channel matrix can not be found, then $\mathbf{u} = \mathbf{0}$ and symbol-level precoding (2) turns into the Zero-Forcing precoding as

$$\mathbf{x}_{zf} = \mathbf{W}_{\text{ZF}}\mathbf{s}. \tag{6}$$

Therefore, the minimal performance of the proposed precoding technique is expected at the level of the Zero-Forcing method in a statistically averaged CSI data. If at least one element of the optimization vector $\mathbf{u}$ is non-zero, then user symbols with an excursion can be constructed to minimize the power of the precoded signal so that ($\|\mathbf{x}\|_2 < \|\mathbf{x}_{zf}\|_2$). Further in the paper, we will refer to the proposed precoding technique as NNLS-SLP.

2.3. Computational Complexity Analysis

The asymptotic computational complexity of the ZF technique is $O(n^3)$ for the channel matrix ($\mathbb{R}^{n\times n}$) inversion operation and $O(n^2)$ for the vector and matrix multiplication per each set of symbols.

The computationally efficient SLP design, described in the previous section, partially uses the same operations as the ZF. The asymptotic computational complexity is $O(n^3)$ for the channel matrix inversion operation and $O(n^2)$ for the vector and matrix multiplication per each set of symbols. The most computationally demanding part of the SLP design is a high-performance algorithm to solve the NNLS optimization problem and find the optimization vector ($\mathbf{u}$), which is executed per every set of symbols. We use the standard fast non-negativity-constrained least squares algorithm (FNNLS) [16, 17], which can be implemented on the Software Defined Radio and FPGA platforms.

We implemented the algorithm using the LabVIEW Communication code to achieve the best computational performance available on the development platform. The most complex operation of such algorithm is solving of unconstrained linear least squares sub-problems via QR decomposition. The asymptotic complexity of the QR decomposition is $O(n^3)$. However, there are more efficient methods that can reduce considerably this level of complexity up to $O(n^2)$ [18], which will be considered in the future for a set-up with a higher number of the transmitters and receivers.

We also show that finding the optimized user symbols $\mathbf{s}+\mathbf{u}$ is equivalent to and more efficient than constructing a precoding matrix $\overline{\mathbf{W}}$ which does not orthogonalize the channel ($\mathbf{H}\overline{\mathbf{W}} \neq \mathbf{I}$). If we are able to find the non-zero solution for the problem (3) then the optimal precoded symbols are calculated as

$$\mathbf{W}_{\mathrm{ZF}}(\mathbf{s}+\mathbf{u}) = \mathbf{x}. \tag{7}$$

Then the left part of the equation (7) can be also expressed as

$$\overline{\mathbf{W}}\mathbf{s} = \mathbf{x}. \tag{8}$$

We can find the appropriate matrix $\overline{\mathbf{W}}$ to satisfy the equality (8) by solving a set of linear equations for the given $\mathbf{s}$ and $\mathbf{x}$. Therefore, finding $\overline{\mathbf{W}}$ is equivalent to solving an optimization problem

$$\begin{aligned} &\min_{\overline{\mathbf{W}}} \|\overline{\mathbf{W}}\mathbf{s}\|_2 \\ &\text{s. t.} |\mathbf{y}| \geq |\mathbf{s}|. \end{aligned} \tag{9}$$

The system defined in (9) has degree of freedom equal to N^2, while the degree of freedom of the system defined in (3) is just N. The later system is much easier to optimize and requires less computational power.

2.4. Impact of the proposed SLP on constellation

Following the previous discussion of the NNLS-SLP algorithm, the figure 1 shows how one symbol of the QPSK constellation can have an amplitude excursion in the positive quadrant space due to the presented optimization vector $\mathbf{u}$. Here we obtain a theoretical BER expression assuming that the receiver recovers perfectly the phase of the reference symbols. This phase recovery may be approached in a realistic scenario by means of repetitive pilot symbols (precoded or not) which are not modified. In addition, an accurate synchronization can be maintained if modified symbols have in average the same phase of the mapping symbols. We reach such a condition by defining the excursion ratio of the mapping symbol as $\epsilon = \mathrm{Re}(u_i)/\mathrm{Re}(s_i)$ for $i = 1, \ldots, N$. The excursion ratio limits the maximum value of $\mathbf{u}$ in respect to the magnitude of the constellation symbols $\mathbf{s}$. For the particular case of a symbol of a QPSK modulation the BER is $p_{\mathbf{es}} = 0.5(\mathcal{Q}(\sqrt{\gamma}) + \mathcal{Q}\left(\sqrt{\gamma}(1+\epsilon)\right))$ where $\mathcal{Q}(\cdot)$ is the standard Gaussian complementary cumulative distribution function, and γ is the SNR, where we assume that the received signal is affected by an additive zero-mean

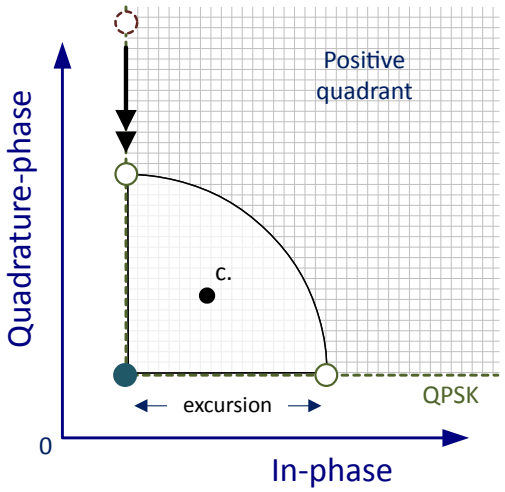

Figure 1: Symbol excursion in NNLS-SLP. The symbol excursion can be in the vertical or horizontal axis.

circulary-symmetric complex Gaussian noise. The ensemble BER is computed to be $0.75\mathcal{Q}(\sqrt{\gamma}) + 0.25\mathcal{Q}(\sqrt{\gamma}(1+\epsilon))$, under the assumption that all symbols have the same probability and half of the symbols have the same amplitude excursion in one dimension and the other half do not have any excursions.

3. Numerical Simulation

3.1. Benchmark System Parameters

We evaluate the performance of the proposed technique and compare it to other benchmark precoding methods, namely ZF and MMSE. We generate 2×2 MIMO channel matrix with a specific 2-norm matrix condition number defined as

$$\kappa_2(\mathbf{H}) = ||\mathbf{H}||_2 \cdot ||\mathbf{H^{-1}}||_2, \tag{10}$$

and injected the AWGN noise. The 2-norm corresponds to the ratio of the largest singular value of that matrix to smallest singular value. By varying 2-norm from low to high values, we perform the benchmark with the channel matrices conditioned from a close-to-diagonal to a close-to-singular and increasing the power imbalance in the channel. The corresponding benchmark measurements for all the techniques performed using the same channel matrix generation.

3.2. Simulated Bit Error Performance of NNLS-SLP

Figures 2 and 3 show the theoretical BER performance of the NNLS-SLP compared to ZF and MMSE techniques. The BER values at each SNR value is

averaged over 10^6 samples. The NNLS-SLP performs better than ZF in terms of improved BER. The advantage of NNLS-SLP over ZF becomes more prominent with the increasing condition number of the channel matrix. In this case the NNLS-SLP technique generates the user symbols with even higher excursion which results in lower BER values (Figure 3). It is noticeable, that NNLS-SLP benchmarks at lower BER than ZF in the whole range of the E_b/N_0 and lower than MMSE techniques for E_b/N_0 higher than 0 dB.

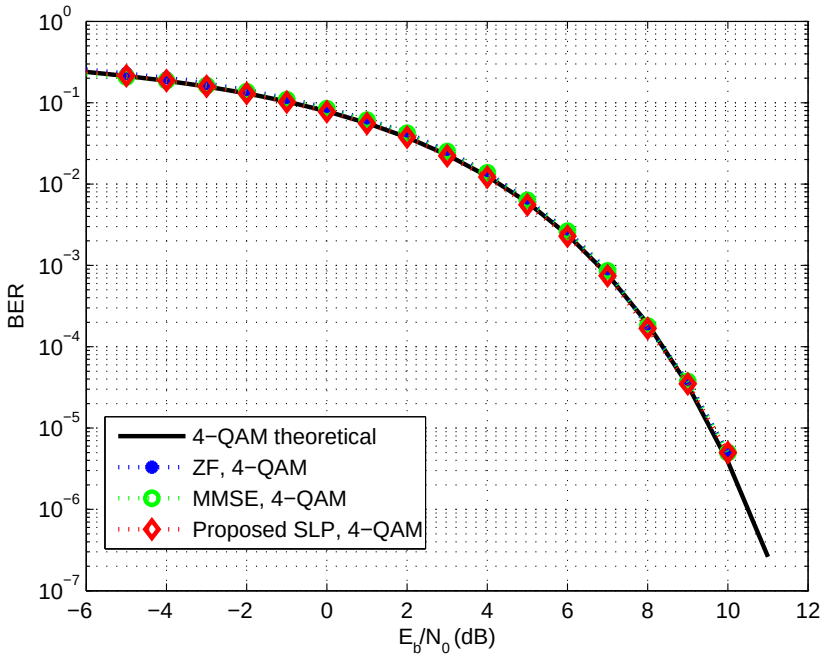

Figure 2: Simulated BER values averaged over 10^6 samples for ZF, MMSE and NNLS-SLP compared to the theoretical 4-QAM BER curve. The perfect compensation of the phase rotation at the receiver is considered. The condition number of the channel matrix is 3.

3.3. Simulated Total Consumed Power of NNLS-SLP

Table 1 shows difference between the total average power of the precoded symbols generated using ZF and NNLS-SLP algorithms. We can see that with the higher channel matrix condition number we generate less total power using the NNLS-SLP algorithm. At the same time we observe an improved Quality of Service over the ZF as we saw in the previous section. At the greater condition number of the channel matrix the power unbalance at the receivers is higher. The interfering signal can be higher in power than the useful signal for the one of the receivers. The occurring inter-user interference can be both constructive and destructive toward the useful signal. The NNLS-SLP technique does not cancel

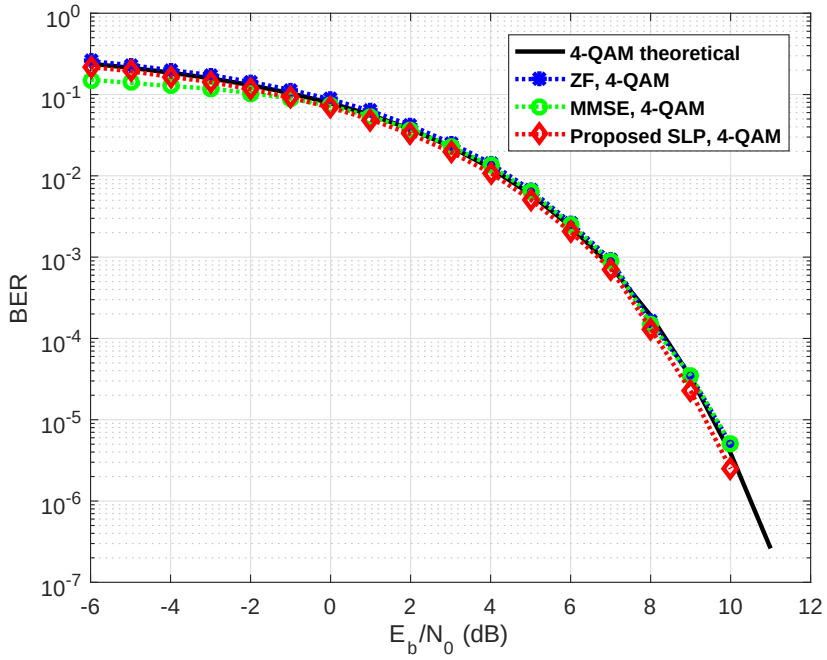

Figure 3: Simulated BER values averaged over 10^6 samples for ZF, MMSE and NNLS-SLP compared to the theoretical 4-QAM BER curve. The perfect compensation of the phase rotation at the receiver is considered. The condition number of the channel matrix is 6.

the components of constructive interference, which provide additional excursion of the mapping symbols and push the symbols deeper into their detection region providing higher BER score. The ZF cancels all the components of interference to have constant mapping symbols, and therefore requires more energy at the transmitter than the NNLS-SLP.

Table 1: Reduction of the total average power of the precoded symbols in 2×2 MIMO system by NNLS-SLP

Matrix condition number	Power reduction
2.5	0.03 dB
3	0.04 dB
3.5	0.07 dB
4	0.09 dB
5	0.35 dB
6	0.72 dB
8	0.88 dB

4. Experimental Validation

4.1. Experimental Setup

In order to demonstrate the feasibility of the proposed SLP technique we build a 2×2 demonstrator with a transmitter, a channel emulator and two receivers using SDR platforms. Figure 4 shows a simplified block diagram of the Precoding demonstrator.

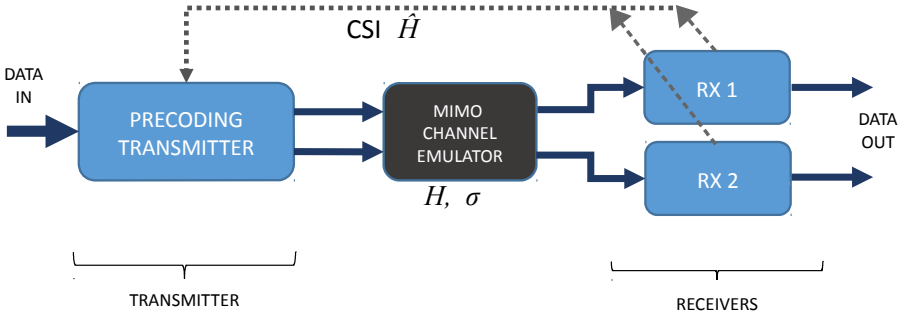

Figure 4: Precoding test bed diagram.

The transmitter performs the ZF and SLP precoding operation using the CSI obtained from the receivers through a return channel. Before precoding, each of the input bit streams are xor-scrambled with different gold sequences obtained from the combinations of the two maximum-length sequences with the characteristic polynomials $1 + x^3 + x^{20}$ and $1 + x^2 + x^{11} + x^{17} + x^{20}$. This scrambling is used in order to obtain a transmission in which all the symbols have the same probability of occurrence. The transmitted data is a set of two different video streams. Table 2 shows a summary of the parameters of the precoded transmitted signals.

Table 2: Experimental parameters of precoded transmission in 2×2 MIMO system

Parameter	Value
Modulation type	QPSK
TX to Emulator c. frequency	1210 MHz
Emulator to RXs c. frequency	960 MHz
Sampling frequency	1 MHz
Over-sampling factor	4
Pulse shaping filter	SRRC with 0.2 roll-off
Pilot duration	24 symbols
Data duration	896 symbols
Pilot repetition period	2048 symbols

The transmitted signals are sent to the MIMO channel emulator, which applies the channel matrix $\mathbf{H}$ and injects to the signals an additive white Gaussian noise with a controlled power. These channel functionalities are implemented in a FPGA which is integrated to the SDR platform. The RF inputs and outputs of the channel emulator operate at different carrier frequencies. Using this configuration we decrease mutual coupling between the transmission and reception links through the RF part of the channel emulator and therefore the accuracy in setting of the desired channel matrix. The channel emulator can generate and apply a 2×2 complex channel matrix with a given condition number and set accurately the power of the AWGN. The channel emulator as well measures the actual output power on each port of the transmitter.

The receivers estimate CSI from the multi-tone pilots, feedback the CSI to the transmitter, recover a waveform and demodulate the signal into information bits. We do not evaluate the mismatch between the the CSI estimation and the actual channel coefficients. To do so we need to compare the estimated CSI to the $\mathbf{H}$ in the hardware channel emulator. Although we know the exact $\mathbf{H}$ values, the channel emulator operates with deviations from these values due to hardware impairments. The receivers calculate BER using the recovered information bits and reference bits. The information bits are streamed to a video playback program. The receivers are programmed on the host using LabVIEW code. The complicated and complex code of receivers is easier and faster to implement in LabVIEW, but it performs significantly slower than FPGA code. Therefore, we had to limit the number of symbols and the modulation order the receivers can process in real-time in a single frame. We show in the table 2 that the pilot repetition period is 2048 symbols, but the actual data duration is only 896 symbols. It is the maximum number of symbols the receivers can process and demodulate before the next frame sequence arrives.

Figure 5 shows a photography of the experimental set-up. We use National Instruments USRP-RIO NI-2944-R as SDR platform. Each of the SDR platforms is controlled by a dedicated PC host. The PCs are also used for data collection, processing and visualization.

4.2. Symbol-Level Optimized Precoding Evaluation

We use the aforementioned experimental environment to benchmark the optimized symbol-level precoding technique. We generate a set of random channel matrices $\mathbf{H}$ with unitary matrix F-norm, defined by $||\mathbf{H}||_{\mathbf{F}} = \text{trace}(\mathbf{H}^H\mathbf{H})$, and for different matrix conditioning numbers, defined by 10.

For each channel matrix generation we apply the NNLS-SLP and compare the results to conventional channel-inversion ZF precoding. In both cases we normalize the precoding matrix to have an unitary 2-norm, so that we obtain a constant value for the expectancy of transmitted power per antenna. Under this constraints, we measured the power in the two receivers and compare the results for different channel realizations for a set of channel matrix conditioning numbers between 2.5 and 4, as is shown in Figures 6 and 7. It is worth to note that in both cases ZF and NNLS-SLP we use the same channel inversion matrix.

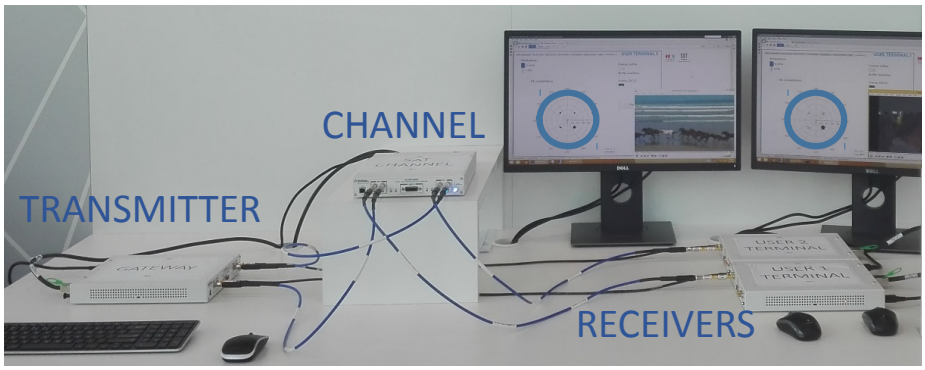

Figure 5: Precoding 2×2 Experimental Settings. The SDR platform used for transmitter, channel emulator and receivers is the NI-2944-R.

However, the difference for NNLS-SLP is the use of optimized symbols, which are limited to the unitary amplitude.

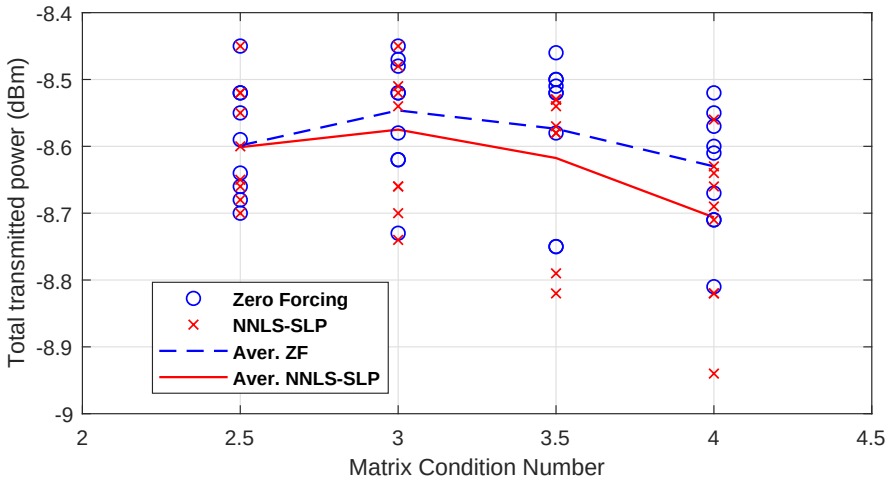

Figure 6: Different realizations of the total transmitted power on 2 output antenna ports, for conventional ZF and NNLS-SLP.

We see in Figure 6 that the Zero-Forcing technique generates signal with a higher averaged total transmitted power than the NNLS-SLP technique. The reduction of the transmitted power by NNLS-SLP is increasing as the matrix condition number increases comparing to ZF. The magnitudes of the power reduction very closely match the theoretically values from the Table 1. By enabling the NNLS-SLP the total power is reduced by 0.03 dB (theoretical - 0.04 dB) at the condition number 3 and by 0.07 dB (theoretical - 0.09 dB) at

the condition number 4.

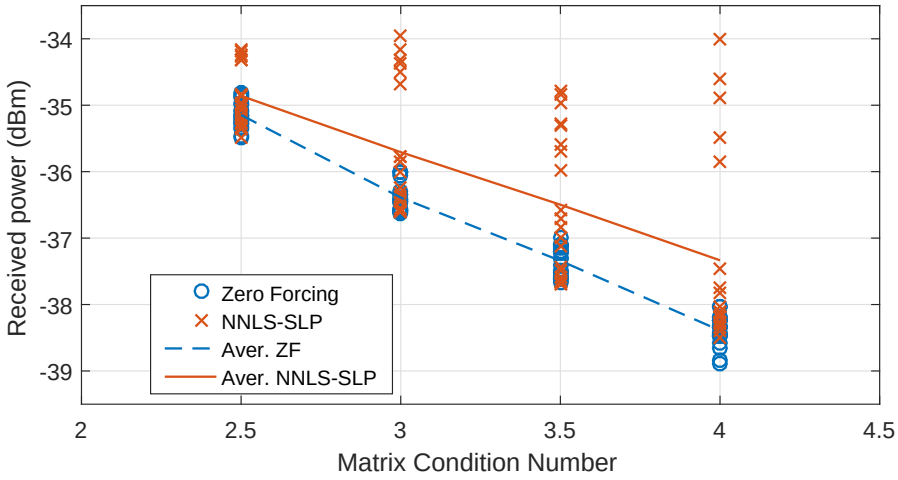

Figure 7: Different realizations of detected power, in 2 receivers indistinctly, for conventional ZF and NNLS-SLP.

From Figure 7 we can observe that the received power for ZF precoding is not a constant for a given conditioning number as should be expected from the theory. These variations come from the imperfections in the actual hardware implementation. Some of these imperfections are the limited accuracy in the CSI estimation, and its quantization error. Nevertheless these imperfections have the same impact on the ZF and the NNLS-SLP, we can observe that the NNLS-SLP has gains in the received power. These gains become more frequent as the matrix conditioning number is increased. There are particular channel realizations in which the NNLS-SLP performs the same as ZF for both receivers, and others realizations in which the optimized symbol is only produced for one of the receivers. Up to this point, we have observed the gains in received power for NNLS-SLP. In the following we will observe how this gain is translated to BER performance in the receiver.

4.3. Bit Error Performance of NNLS-SLP

Figure 8 shows an example of received modified constellation with the NNLS-SLP algorithm with some AWGN already applied. This constellation will be difficult to demodulate by a conventional QPSK demodulator as the one used (LabVIEW Communications v.2.0), as the phase synchronization algorithm tracks for the mean square phase error, which is increased in the proposed constellation. However, the symbol excursion will help for the cases in which the phase is correctly recovered and also for very low SNR conditions in which the received signal is very affected by additive noise. For this reason we proceed to perform BER experiments for different SNR values.

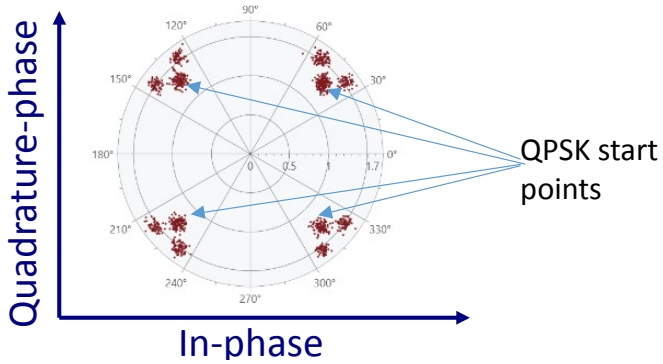

Figure 8: An example of NNLS-SLP modified received constellation.

The SNR is set by means of the injection of artificial AWGN in the channel emulator. The noise power can be accurately controlled to adjust the desired SNR, knowing the exact value of the received signal power. First, we performed a single link BER measurement using an unmodified QPSK constellation. We use it as a reference to evaluate the effects of imperfect phase synchronization for low SNR values. Phase-locked loop of the demodulator is reset for every frame. For the case of NNLS-SLP the precoded pilot symbols are not modified from the QPSK original mapping points.

We performed measurements of BER for ZF and NNLS-SLP for different channel matrices, where the SNR was estimated using ZF precoding. This is a fair comparison, since, despite the average received power can increase while using NNLS-SLP, minimal received power can still match the one gained with ZF precoding for some symbols. Figure 9 shows the theoretical ideal QPSK BER values, the BER for a single non-interference link, and the BER for ZF and NNLS-SLP for a particular matrix with conditioning number 2.5 which gives and excursion (in horizontal and vertical axis) of 4%.

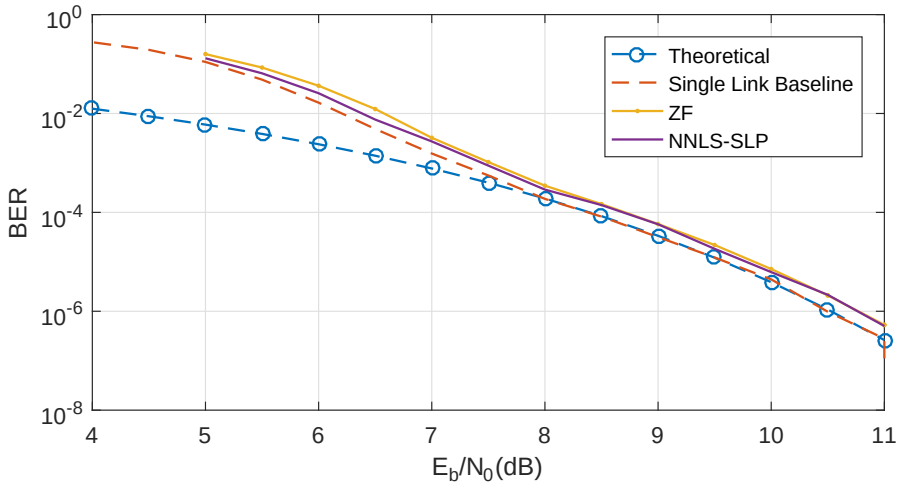

Figure 9: Experimental BER plots for ZF and NNLS-SLP compared to an experimental baseline non-interference QPSK BER and to the theoretical BER curve. The matrix condition for the precoded channel is 2.5. The NNLS-SLP in this case provides an excursion of 4%. Only a slight degradation is seen in the precoded system, which carries twice the data rate using the same frequency band.

Here we see a degradation of the BER plots which use precoding compared to the single link BER curve. This is attributed to the inaccuracies in the CSI estimation, which produces residual interference that affects the BER performance, however, we should remark that for the case of precoded signals we obtain twice spectral efficiency, since the system provide two separate streams using the same frequency band. We showed that the NNLS-SLP perform better than ZF for low SNR values, and that the ZF perform better at some points of higher SNR values using a conventional receiver. The experiment is repeated with some channel matrices with higher proposed excursion values which in some cases gives a degradation in BER performance for high SNR values. Most of these errors are due to the lack of phase synchronization and phase tracking. These effects can be observed as a rotated shaking in the constellation plots in the graphical user interface at the receiver.

It is worth to clarify that, at the transmitter QPSK modulator maps the transmitted symbols in correspondence to optimization excursion from the NNLS-SLP. However, at the receiver QPSK demodulator normalizes the received symbols in correspondence to conventional QPSK symbol map.

Figure 10 shows the BER curves for for ZF and NNLS-SLP for a particular matrix with conditioning number of 3 which gives and excursion (in horizontal and vertical axis) of 20%. Here we can observe how the NNLS-SLP scores lower SNR than the conventional ZF for E_b/N_0 values lower than 8 dB.

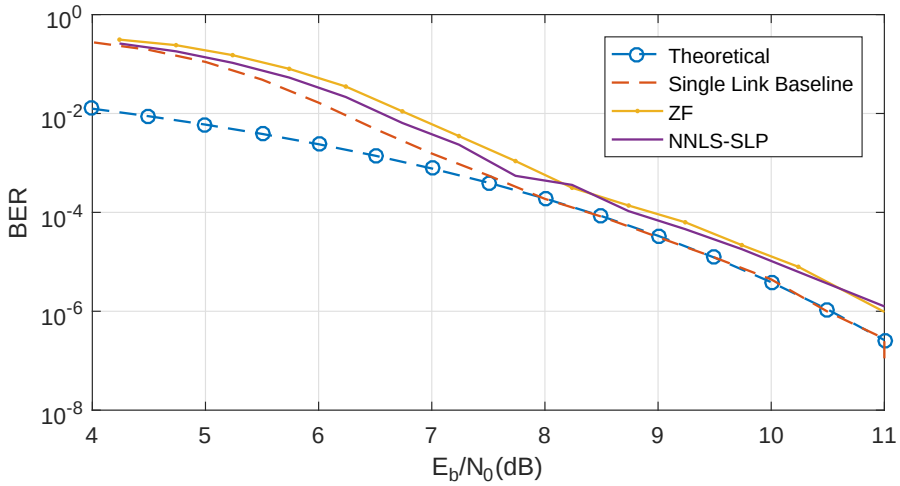

Figure 10: Experimental BER plots for ZF and NNLS-SLP compared to a experimental baseline QPSK BER and to the theoretical BER curve. The matrix condition number for the precoded channel is 3 The NNLS-SLP in this case provides an excursion of 20%.

5. Conclusions

In this paper, we presented the theoretical and experimental results using the hardware demonstration of precoded satellite communications based on state-of-art SLP technique. The SLP beamforming benchmarked similar BER results to ZF beamforming in the case scenario of high SNR. However, it is experimentally proven that NNLS-SLP technique takes advantages of unbalanced channel matrices with strong interference components to increase received signal SNR, improve service quality and minimize the transmit power at the gateway.

Therefore, we evidently shown that SLP technique can provide better SNR performance than conventional ZF technique in real-time transmissions for low SNR scenarios. The theoretical simulation data predicted improvement of the BER performance for high SNR scenarios. However, a decrease in the BER performance was observed in the experimental data. This performance decrease, which is generated by an imperfection in the carrier synchronization and tracking can be avoid if global synchronization is achieved. Some of examples of this are the multi-carrier or OFDM systems in which many carriers are jointly synchronized and aided by additional synchronization carrier pilots. Another example in which this method can be applied is in the low SNR regimes of single carrier communications which maintain phase coherency along time, such as the satellite communication standards as DVB-S2X, where the receiver synchronization is improved over longer averaging periods. In addition, the improvements for the evaluated method will increase with higher order MIMO systems, where the gains obtained from the symbol-level optimization can increase.

We demonstrated, that the condition number of the channel matrix has an impact on the performance of the NNLS-SLP technique in theoretical and experimental benchmarks. At the greater condition number of the channel matrix the power unbalance at the receivers is higher, which enables the NNLS-SLP technique to exploit occurring constructive interference between the users.

In this paper we also demonstrate, to the best author knowledge, the first symbol-level optimized precoded communication system, in a real hardware implementation. We show experimentally the feasibility of the proposed SLP in terms of complexity and energy efficiency.

Acknowledgements

This research was supported by Luxembourg National Research Fund grant for "SERENADE" project and AFR-PPP "End-to-end Signal Processing Algorithms for Precoded Satellite Communications" project.

References

[1] W. Zeng, C. Xiao, M. Wang, J. Lu, Linear precoding for finite-alphabet inputs over mimo fading channels with statistical csi, IEEE Transactions on Signal Processing 60 (6) (2012) 3134–3148. doi:10.1109/TSP.2012.2188717.

[2] N. Song, T. Yang, M. Haardt, Efficient hybrid space-ground precoding techniques for multi-beam satellite systems, in: 2017 IEEE International Conference on Acoustics, Speech and Signal Processing (ICASSP), 2017, pp. 6284–6288. doi:10.1109/ICASSP.2017.7953365.

[3] Q. H. Spencer, A. L. Swindlehurst, M. Haardt, Zero-forcing methods for downlink spatial multiplexing in multiuser mimo channels, IEEE Transactions on Signal Processing 52 (2) (2004) 461–471. doi:10.1109/TSP.2003.821107.

[4] X. Artiga, M. A. Vazquez, A. Perez-Neira, C. Tsinos, E. Lagunas, S. Chatzinotas, V. Ramireddy, C. Steinmetz, R. Zetik, K. Ntougias, D. Ntaikos, C. B. Papadias, Spectrum sharing in hybrid terrestrial-satellite backhaul networks in the ka band, in: 2017 European Conference on Networks and Communications (EuCNC), 2017, pp. 1–5. doi:10.1109/EuCNC.2017.7980751.

[5] R. B. Moraes, P. Tsiaflakis, J. Maes, M. Moonen, General framework and algorithm for data rate maximization in dsl networks, IEEE Transactions on Communications 62 (5) (2014) 1691–1703. doi:10.1109/TCOMM.2014.030214.130507.

[6] S. Neshvad, S. Chatzinotas, J. Sachau, Wideband identification of power network parameters using pseudo-random binary sequences on power inverters, IEEE Transactions on Smart Grid 6 (5) (2015) 2293–2301. doi:10.1109/TSG.2015.2397552.

[7] C. B. Peel, B. M. Hochwald, A. L. Swindlehurst, A vector-perturbation technique for near-capacity multiantenna multiuser communication-part i: channel inversion and regularization, IEEE Transactions on Communications 53 (1) (2005) 195–202. doi:10.1109/TCOMM.2004.840638.

[8] E. Björnson, M. Bengtsson, B. E. Ottersten, Optimal multiuser transmit beamforming: A difficult problem with a simple solution structure, CoRR abs/1404.0408.
URL http://arxiv.org/abs/1404.0408

[9] D. Christopoulos, S. Chatzinotas, I. Krikidis, B. E. Ottersten, Constructive Interference in Linear Precoding Systems: Power Allocation and User Selection, CoRR abs/1303.7454.
URL http://arxiv.org/abs/1303.7454

[10] A. Kalantari, C. G. Tsinos, M. Soltanalian, S. Chatzinotas, W. Ma, B. E. Ottersten, Energy-efficient M-QAM precoder design with spatial peak power minimization for MIMO directional modulation transceivers, CoRR abs/1702.06878.
URL http://arxiv.org/abs/1702.06878

[11] Y. C. B. Silva, A. Klein, Linear Transmit Beamforming Techniques for the Multigroup Multicast Scenario, IEEE Transactions on Vehicular Technology 58 (8) (2009) 4353–4367. doi:10.1109/TVT.2009.2021603.

[12] C. Masouros, E. Alsusa, Dynamic linear precoding for the exploitation of known interference in MIMO broadcast systems, IEEE Transactions on Wireless Communications 8 (3) (2009) 1396–1404. doi:10.1109/TWC.2009.080053.

[13] P. B. Ottersten, D. S. Chatzinotas, D. S. Andrenacci, D. J. M. Duncan, D. M. Alodeh, Serenade: Satellite precoding hardware demonstrator (2017).
URL https://wwwfr.uni.lu/snt/technology_transfer_office/success_stories/serenade_satellite_precoding_hardware_demonstrator

[14] J. C. Merlano-Duncan, J. Krivochiza, S. Andrenacci, S. Chatzinotas, B. Ottersten, Computationally efficient symbol-level precoding communications demonstrator, in: 2017 IEEE 28th Annual International Symposium on Personal, Indoor, and Mobile Radio Communications (PIMRC), 2017.

[15] J. Krivochiza, A. Kalantari, S. Chatzinotas, B. Ottersten, Low complexity symbol-level design for linear precoding systems, in: 2017 Symposium on

Information Theory and Signal Processing in the Benelux, Delft University of Technology, 2017, p. 117.

[16] C. Lawson, R. Hanson, Solving Least Squares Problems, Society for Industrial and Applied Mathematics, 1995. arXiv:http://epubs.siam.org/doi/pdf/10.1137/1.9781611971217, doi:10.1137/1.9781611971217.
URL http://epubs.siam.org/doi/abs/10.1137/1.9781611971217

[17] R. Bro, S. De Jong, A Fast Non-negativity-constrained Least Squares Algorithm, Journal of Chemometrics 11 (5) (1997) 393–401. doi:10.1002/(SICI)1099-128X(199709/10)11:5<393::AID-CEM483>3.0.CO;2-L.

[18] Y. Luo, R. Duraiswami, Efficient parallel nonnegative least squares on multicore architectures, SIAM Journal on Scientific Computing 33 (5) (2011) 2848–2863. arXiv:https://doi.org/10.1137/100799083, doi:10.1137/100799083.
URL https://doi.org/10.1137/100799083